ELSEVIER

Chemical Engineering Journal 137 (2008) 23–29

Chemical Engineering Journal

www.elsevier.com/locate/cej

Biocompatible mesoporous silica nanoparticles with different morphologies for animal cell membrane penetration

Brian G. Trewyn, Jennifer A. Nieweg, Yannan Zhao, Victor S.-Y. Lin *

Department of Chemistry and U.S. DOE Ames Laboratory, Iowa State University, Ames, IA 50011-3111, USA

Received 30 May 2007; received in revised form 22 September 2007; accepted 24 September 2007

Abstract

Two MCM-41 type, fluorescein-labeled mesoporous silica nanomaterials (MSNs) consisting of spherical and tube-shaped particles were synthesized and characterized. Both materials have hexagonally arranged mesopores with high surface area (>950 m^2/g) and a narrow distribution of pore diameters. The cellular uptake efficiency and kinetics of both MSNs were measured in a cancer cell line (CHO) and a noncancerous cell line (fibroblasts) by flow cytometry and fluorescence confocal microscopy. The correlation between the particle morphology and aggregation of MSNs to the effectiveness of cellular uptake was investigated. We envision that our study on the morphology dependent endocytosis of MSNs would lead to future developments of efficient transmembrane nanodevices for intracellular sensing and gene/drug delivery.

Keywords: Mesoporous silica nanoparticle; Endocytosis; Nanosphere; Nanotube; Cell membrane; Intracellular delivery

1. Introduction

Since the discovery of surfactant-templated synthesis of mesoporous silica materials in 1992 [1,2], many reports in the literature have explored the functionalization and utilization of these structurally ordered materials for applications in a variety of areas, such as catalysis [3–5], separation [6,7], and sensor [8,9]. The unique properties, such as high surface area (>700 $m^2\ g^{-1}$), large pore volume (>0.9 $cm^3\ g^{-1}$), tunable pore size with a narrow distribution (2–10 nm), and good chemical and/or thermal stability, of these silica materials also make them potentially suitable for several important biological applications, such as drug delivery, imaging, and controlled release/sequestration [10–16].

While several research groups worldwide have investigated the controlled release properties of various mesoporous silica materials, the amorphous nature of these materials make them difficult to handle under physiological conditions. The random aggregation of the amorphous and polydisperse particles of mesoporous silicas in aqueous solutions with high ionic strength complicates their circulation lifetime and cell membrane permeability. Because of these issues, it is difficult to predict and regulate the biocompatibility of amorphous mesoporous silica materials both in vitro and in vivo. In contrast, surface-functionalized solid silica particles with spherical shape and narrow size distribution have been used for biological applications [17–20].

To construct mesoporous silica-based functional materials for practical applications in biotechnology and biomedicine, the ability to control the particle morphology and surface properties of these materials is of fundamental importance. Several recent reports on the morphological control and surface functionalization of mesoporous silica nanoparticle (MSN) materials have shown promising results in improving their in vitro biocompatibility and cell membrane permeability [9,21–24]. In particular, the recent demonstrations on the endocytosis of these MSN particles into animal and plant cells highlight the possibility of designing nanodevices for controlling cell membrane traffic [23], which would allow efficient deliveries of a variety of biogenic molecules into cell bodies.

To date, only spherical MSNs with an average particle size around 100–200 nm have been investigated for the endocytosis of live cells [23]. To further advance this burgeoning field of research, it is important to gain fundamental insight on how the different shapes and particle sizes would impact the cell membrane permeability of mesoporous silica materials. Herein, we report on the synthesis and characterization of two kinds of mesoporous silica particles with spherical and tube-like mor-

* Corresponding author. Tel.: +1 515 294 3135.
E-mail address: vsylin@iastate.edu (V.S.-Y. Lin).

1385-8947/$ – see front matter © 2007 Elsevier B.V. All rights reserved.
doi:10.1016/j.cej.2007.09.045

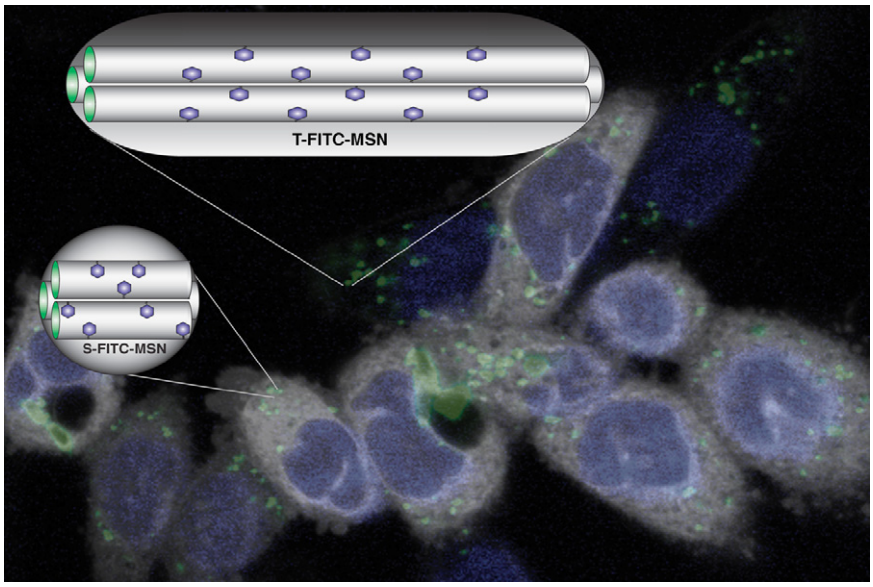

Fig. 1. Schematic representation of cell uptake and internalization of spherical and tube-shaped FITC-MSN.

phologies. The cellular uptake efficiency and kinetics were measured and compared to particle size and aggregation occurrence in aqueous buffer, as depicted in Fig. 1. We discovered that cancer cells endocytosed both MSNs more efficiently and at a faster rate than fibroblast cells. We also discovered that the rate of endocytosis correlates with the degree of particle aggregation.

2. Experimental

2.1. Synthesis of spherical fluorescein isothiocyanate-doped MSNs (S-FITC-MSN)

The MSN material was prepared by the following procedures: First, 1.0 mg fluorescein isothiocyanate was stirred for 30 min at room temperature with 5.0 μL 3-aminopropyltrimethoxysilane (APTMS) in 500.0 μL anhydrous DMF. Next, *n*-cetyltrimethylammonium bromide (CTAB, 1.0 g, 2.7×10^{-3} mol) was dissolved in 480.0 mL nanopure water. This solution was made basic by the addition of 3.5 mL 2.0 M NaOH, followed by adjusting the solution temperature to 353 K. Tetraethyl orthosilicate (TEOS) (5.0 mL, 2.6×10^{-3} mol) was first introduced dropwise to the CTAB-containing solution, followed by the dropwise addition of the FITC-APTMS/DMF solution. The mixture was stirred for 2 h at 353 K to give rise to orange precipitates (as synthesized S-FITC-MSNs). The solid product was filtered, washed with deionized water and methanol, and dried under high vacuum at 353 K. To remove the surfactant template (CTAB), the as-synthesized FITC-MSN (1.0 g) was refluxed for 18 h in a solution of 1.0 mL of HCl (37.4%) and 100.0 mL of methanol, followed by washing with methanol and water. The surfactant-removed FITC-MSNs (washed S-FITC-MSNs) were placed under high vacuum to remove solvent from the mesopores, shown previously to remove surfactant to completion by ^{13}C solid state NMR [25]. The amount of fluorescein incorporated to the mesoporous material was determined to be $1.3 \pm 0.5 \times 10^{-4}$ mol/g by ^{29}Si direct polarization solid-state NMR using a previously reported method [25,28].

2.2. Synthesis of tube-shaped fluorescein isothiocyanate-doped MSNs (T-FITC-MSN)

The MSN material was prepared by the following procedures: First, fluorescein isothiocyanate (2.0 mg) was stirred for 30 min at room temperature with 500.0 mL 3-aminopropyltrimethoxysilane (APTMS) in 500.0 mL anhydrous DMF. Next, n-cetyltrimethylammonium bromide (CTAB, 2.0 g, 5.5×10^{-3} mol) was dissolved in 480.0 mL nanopure water. This solution was made basic by the addition of 7.0 mL 2.0 M NaOH, followed by adjusting the solution temperature to 353 K. TEOS (10.0 mL, 5.1×10^{-3} mol) was first introduced quickly to the CTAB-containing solution, followed by the rapid addition of the FITC-APTMS/DMF solution. The mixture was stirred for 2 h at 353 K to give rise to orange precipitates (as synthesized T-FITC-MSN). The solid product was filtered, washed with deionized water and methanol, and dried in under high vacuum at 353 K. To remove the surfactant template (CTAB), the as-synthesized FITC-MSN (1.0 g) was refluxed for 18 h in a solution of 1.0 mL of HCl (37.4%) and 100.0 mL of methanol, followed by washing with methanol and water. The surfactant-removed FITC-MSNs (washed T-FITC-MSN) were placed under high vacuum to remove solvent from the mesopores. The amount of fluorescein incorporated to the mesoporous material was determined to be $1.1 \pm 0.6 \times 10^{-4}$ mol/g by ^{29}Si direct polarization solid-state NMR using a previously reported method [25,28].

2.3. Reagents and materials for biological studies

Chinese Hamster Ovarian (CHO) and Human fibroblast cell lines were obtained from American Tissue Culture Collection

(ATCC). Formaldehyde solution (37%, w/w) was purchased from Fisher. 4,6-Diamidino-2-phenylindole, dihydrochloride (DAPI) and trypan blue were purchased from Sigma–Aldrich. Trypsin (1×, 0.25%) in 0.1% EDTA-Na without calcium and magnesium was purchased from Fisher Scientific.

2.4. Cell line maintenance

CHO and fibroblast cells were maintained in T75 flasks using DMEM (Dulbucco's modified Eagle's medium) supplemented with 10% equine serum, 2 mM L-glutamine, 100 U mL^{-1} penicillin, 100 mg mL^{-1} streptomycin, and 1 mg mL^{-1} gentamycin. CHO and fibroblast cells were split every 2–3 days.

2.5. Measuring the dosage of spherical-FTIC-MSN and tubular-FTIC-MSN uptake

To investigate the maximum amount of material that can be incorporated by CHO and fibroblast cells, a dosage experiment was designed. The cells were grown in 6-well plates for 24 h or until visual confluency developed. The cells were then treated with incremental amounts of T-FITC-MSN and S-FITC-MSN suspended in media. Experiments were designed for both T-FITC-MSN and S-FITC-MSN with concentrations of 0, 5, 10, 25, 50, and 100 μg mL^{-1}. The cells were incubated with the different concentrations of MSNs for 12 h at 37 °C in 5% CO_2. After 12 h, the cells were washed two times with PBS (phosphate-buffered saline) and trypsinized. The cells were incubated in 830 mM trypan blue for 10 min to quench the fluorescence of any MSNs adhered to the exterior of the cells. The MSN uptake was measured by flow cytometry.

2.6. Measuring the kinetics of spherical-FTIC-MSN and tubular-FTIC-MSN uptake

To investigate the rate of MSN uptake into CHO and fibroblast cells, a kinetic experiment study was conceived. The cells were grown in 6-well plates for 24 h, or until visual confluency developed. The cells were incubated with a uniform amount of MSNs (50 μg mL^{-1}) for varying amounts of time. Uptake was measured at 0, 10, 30, 60, 180, and 360 min time intervals. After the pre-determined amount of time, the cells were washed twice with PBS, and incubated in standard growth media. Fourteen hours after initial inoculation, the cells were trypsinized, and the MSN uptake was measured by flow cytometry.

2.7. Fluorescence confocal microscopy measurements

To visually investigate the endocytosis of T-FITC-MSN and S-FITC-MSN, fluorescence confocal microscopy was employed. Coverslips (22 mm^2) were cleaned with 1.0 M HCl, nanopure water (3×), 50% ethanol, 70% ethanol, and 100% ethanol, and dried overnight at 60 °C. Following cleaning, the coverslips were placed on the bottom of the wells of 6-well plates and covered with 3.0 mL of standard growth media. CHO (1.0×10^5 cells mL^{-1}) were grown for 24 h on the coverslips. After 24 h, the cells were inoculated with 50.0 μg mL^{-1} MSNs, and grown for an additional 12 h. Afterwards, the growth media was removed, the cells were washed with PBS (2×), and the cells were then reincubated with a PBS solution of 3.7% formaldehyde and 57.0 mM DAPI for 30 min. These coverslips were removed from the PBS solution and fixed to glass slides with liquid adhesive.

2.8. Nitrogen adsorption/desorption isotherms

Surface analysis of the T- and S-FITC-MSN materials was performed by nitrogen sorption isotherms in a Micromeritics Tristar 3000 sorptometer. The surface areas were calculated by the Brunauer–Emmett–Teller (BET), and the pore size distribution was calculated by the Barrett–Joyner–Halenda method.

2.9. X-ray diffraction measurement

X-ray diffraction patterns of the MSN materials were obtained in a Scintag XDS-2000 powder diffractometer using Cu Kα irradiation. Both materials possess a hexagonal structure

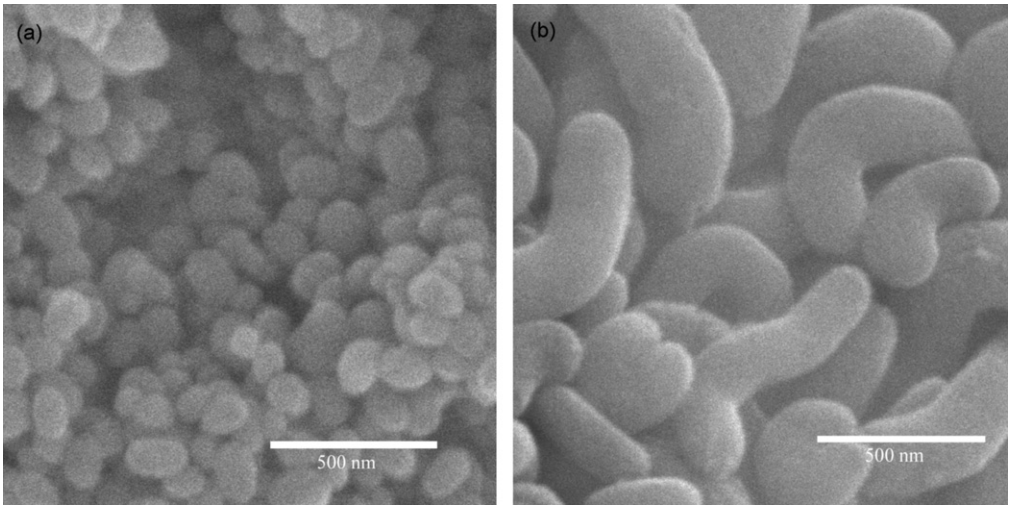

Fig. 2. Scanning electron micrographs of S-FITC-MSN (a) and T-FITC-MSN (b), giving evidence of morphology control during MSN synthesis.

typical of MCM-41 with three characteristic d_{100}, d_{110}, and d_{200} peaks.

2.10. ζ-Potential measurement

The ζ-potential of the MSN materials was measured in a Malvern Nano HT Zetasizer. Five hundred micrograms per milliliter suspensions of each of the materials in phosphate buffer saline buffer were prepared. The pH 7.5 buffer was composed of 2.7 mM KCl, 1.5 mM KH_2PO_4, 136.0 mM NaCl and 8.1 mM $Na_2HPO_4{\cdot}7H_2O$ in nanopure water.

2.11. Scanning and transmission electron microscopy

Particle morphology was studied with a JEOL 840A scanning electron microscope with a 10 kV acceleration voltage. For transmission electron microscopy measurements, an aliquot of the powder was sonicated in nanopure water for 15 min. A single drop of this suspension was placed on a lacey carbon coated copper TEM grid and dried in air. The TEM examination was completed on a Tecnai G2 F20 electron microscope operated at 200 kV to examine at electron optical magnification of 64,000 to 550,000.

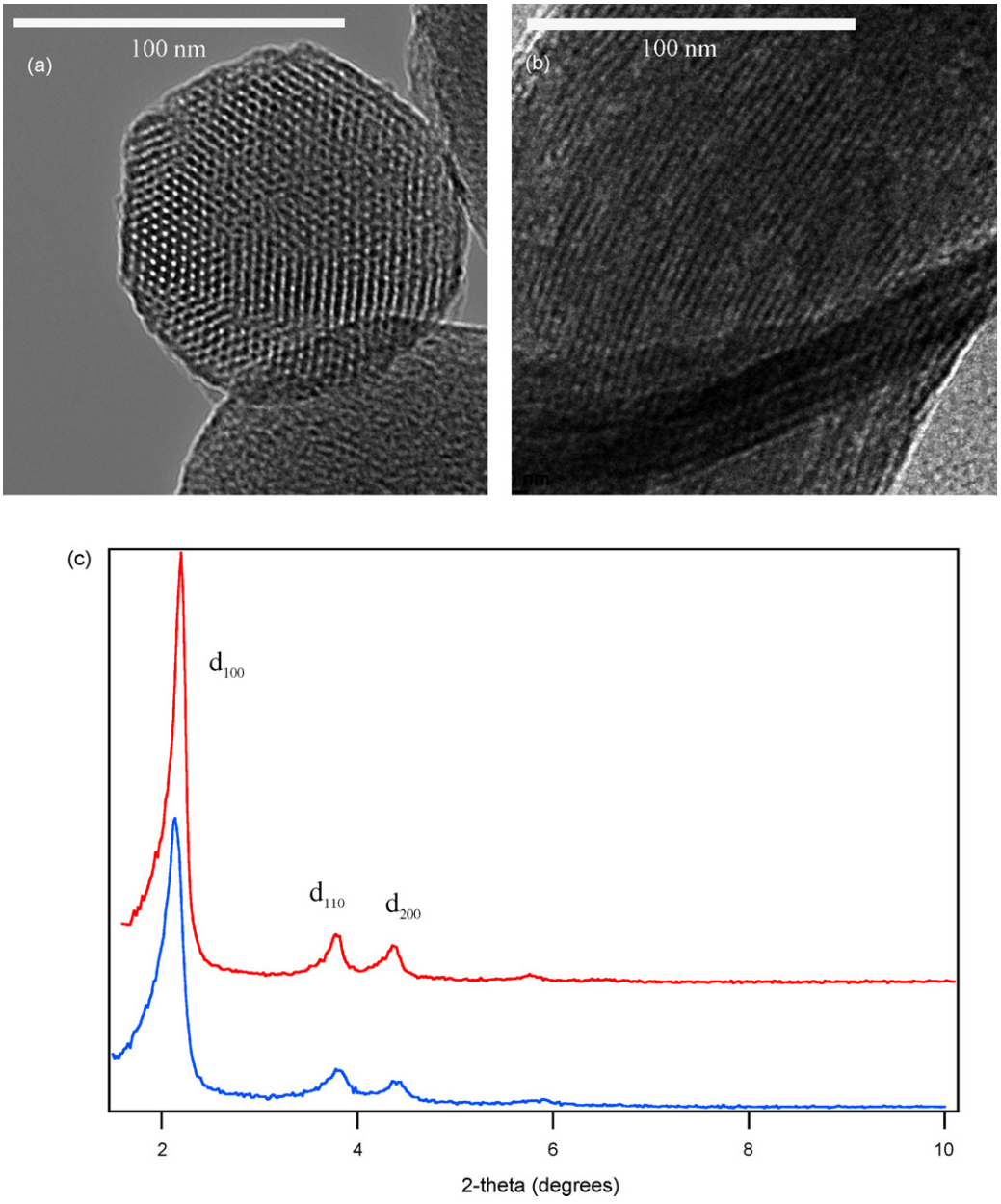

Fig. 3. Transmission electron micrographs of S-FITC-MSN (a) and T-FITC-MSN (b), showing respective particle morphologies at high magnification, and the internal mesopore structure. Low angle X-ray diffraction spectra (c) of S-FITC-MSN (blue) and T-FITC-MSN (red) measured after surfactant-template removal verifying hexagonal mesopore structures. (For interpretation of the references to colour in this figure legend, the reader is referred to the web version of the article.)

3. Results and discussion

To prepare morphology controlled MSNs functionalized with fluorescein, we first reacted FITC with an aminopropyltrimethoxysilane in dry DMF to yield a trimethoxysilylated FITC. By using this compound as a precursor, a tube-shaped, FITC-labeled MSN and a spherical FITC-labeled MSN were successfully synthesized via our recently reported co-condensation method [8,25]. As shown in the SEM micrographs (Fig. 2a), the S-FITC-MSN is indeed a monodisperse material consisting of spherical particles and has a narrow size distribution ranging from 80 to 150 nm in particle diameter. On the other hand, the SEM image of T-FITC-MSN confirmed the tube-like particle morphology with an average particle size of 600 nm in length and 100 nm in width (Fig. 2b). Upon removal of the surfactant template via acid/methanol extraction, both T- and S-FITC-MSNs comprised of MCM-41-type, hexagonally arranged pores as determined by TEM (Fig. 3a and b) and low angle powder XRD (Fig. 3c). Powder XRD analysis confirms hexagonally arranged mesopores in the diffraction pattern of both MSN as evident by the intense d_{100} peak, along with a well-resolved d_{110} and d_{200} (Fig. 3c). Nitrogen sorption analysis of both materials exhibited a Type-IV isotherm, typical of mesoporous material with BET surface areas measured at 951.7 ± 3.0 and $991.2 \pm 3.8\ m^2/g$ for T-FITC-MSN and S-FITC-MSN (Fig. 4), respectively. The average pore diameters were determined to be 27 Å for both materials by the BJH method (Fig. 4 inset).

The cellular uptake of both materials was analyzed by flow cytometry. Both materials were covalently labeled with fluorescein as a fluorescent marker to determine the number of cells that internalized S-FITC-MSN and T-FITC-MSN. Flow cytometry measures the fluorescence of individual cells and counts the number of cells that are above the cellular autofluorescence at each concentration of MSN. As the dosage of MSN increased, the number of cells showed a positive FITC signal also increased. We discovered that the uptake of MSN was both morphology and cell line dependent. Both materials showed more efficient uptake in the cancer cell line (CHO) than fibroblast cells (Fig. 5a). In fact, T-FITC-MSN showed 100% efficient endocytosis between 50.0 and 100.0 $\mu g\ mL^{-1}$ with an EC_{50} of 4.6 $\mu g\ mL^{-1}$, while S-FITC-MSN did not reach 100% efficient endocytosis below the highest measured concentration of 100.0 $\mu g\ mL^{-1}$ and an EC_{50} of 56.0 $\mu g\ mL^{-1}$. However, both materials showed less efficient endocytosis for fibroblast cells (Fig. 5b). In fact, neither material reached 100% efficiency in fibroblast cells; specifically, T-FITC-

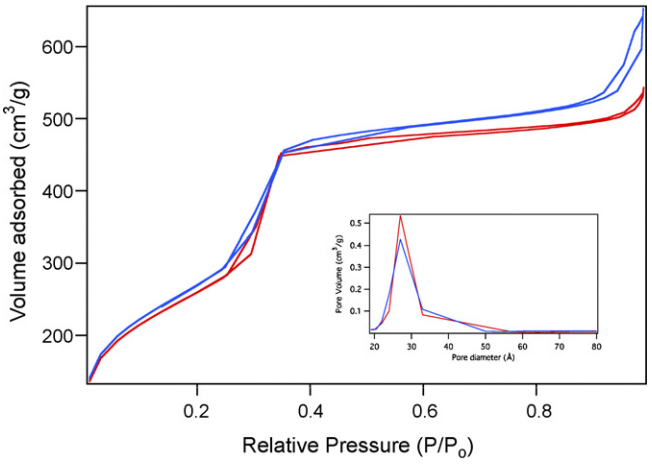

Fig. 4. BET nitrogen adsorption/desorption isotherms of S-FITC-MSN (blue) and T-FITC-MSN (red). BJH pore size distribution of S-FITC-MSN (blue) and T-FITC-MSN (red) (inset). (For interpretation of the references to colour in this figure legend, the reader is referred to the web version of the article.)

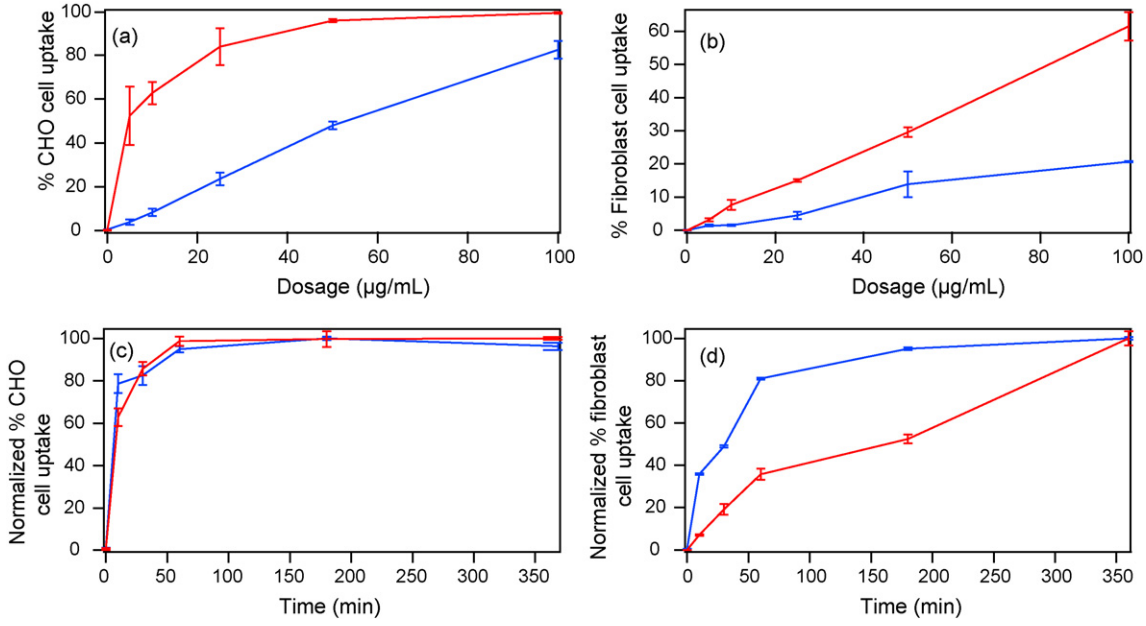

Fig. 5. Dosage efficiency and kinetic measurements in CHO and fibroblast cells S-FITC-MSN (blue) and T-FITC-MSN (red). Dosage efficiency of CHO (a) and fibroblast cells (b) measured after 12 h incubation at 37 °C. Normalized endocytosis kinetics of CHO (c) and fibroblast cells (d) of 50 $\mu g\ mL^{-1}$ incubated at 37 °C. (For interpretation of the references to colour in this figure legend, the reader is referred to the web version of the article.)

MSN reached ~60% efficiency at 100.0 μg mL^{-1} with an EC_{50} of 82.0 μg mL^{-1}. S-FITC-MSN seemed to reach a maximum efficiency at 100.0 μg mL^{-1}, where 21% of the fibroblast cells showed uptake of spherical MSN. To avoid false positives, trypan blue was incorporated in the flow cytometry measurements to quench the fluorescence of MSN that were not internalized but may be attached to the outside of the cell.

In addition to investigating the efficiency of endocytosis, the kinetics of endocytosis for both MSNs was studied. We discovered that the rates of endocytosis for both MSNs were similar and rapid for CHO cells (Fig. 5c). However, the rates of endocytosis for fibroblast cells were different for the MSN with different morphologies. Specifically, the rate of endocytosis for S-FITC-MSN was significantly faster than that of T-FITC-MSN. In the case of S-FITC-MSN, the endocytosis reached nearly 100% uptake in 180 min, while T-FITC-MSN required 360 min to reach 100% endocytosis. This difference in endocytosis kinetics may be attributed to two variables. One is the particle size, S-FITC-MSN are much smaller as is evident from the SEM and TEM analyses (Figs. 2a and 3a). The particle size of S-FITC-MSN is on the order of 80–150 nm in diameter, while T-FITC-MSN have a similar width of 80–150 nm but can vary in length. SEM and TEM data revealed that T-FITC-MSN could reach 400–1000 nm in length. This size variation may account for the difference in the rate of MSN endocytosis.

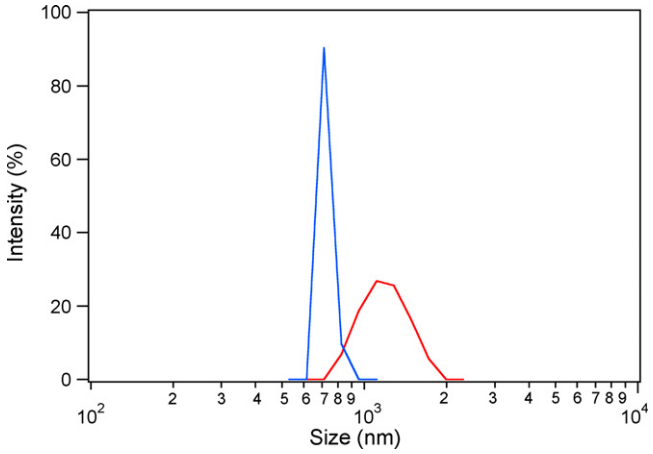

Fig. 6. Dynamic light scattering data of S-FITC-MSN (blue) and T-FITC-MSN (red) measured at a concentration of 500 μg mL^{-1} in PBS. (For interpretation of the references to colour in this figure legend, the reader is referred to the web version of the article.)

The other variable, which can also explain the difference in endocytosis kinetics, is the different aggregation ability between the MSN particles with different shapes. We have previously demonstrated that the uptake of S-FITC-MSN is a clathrin-mediated endocytosis process [23] and there are numerous

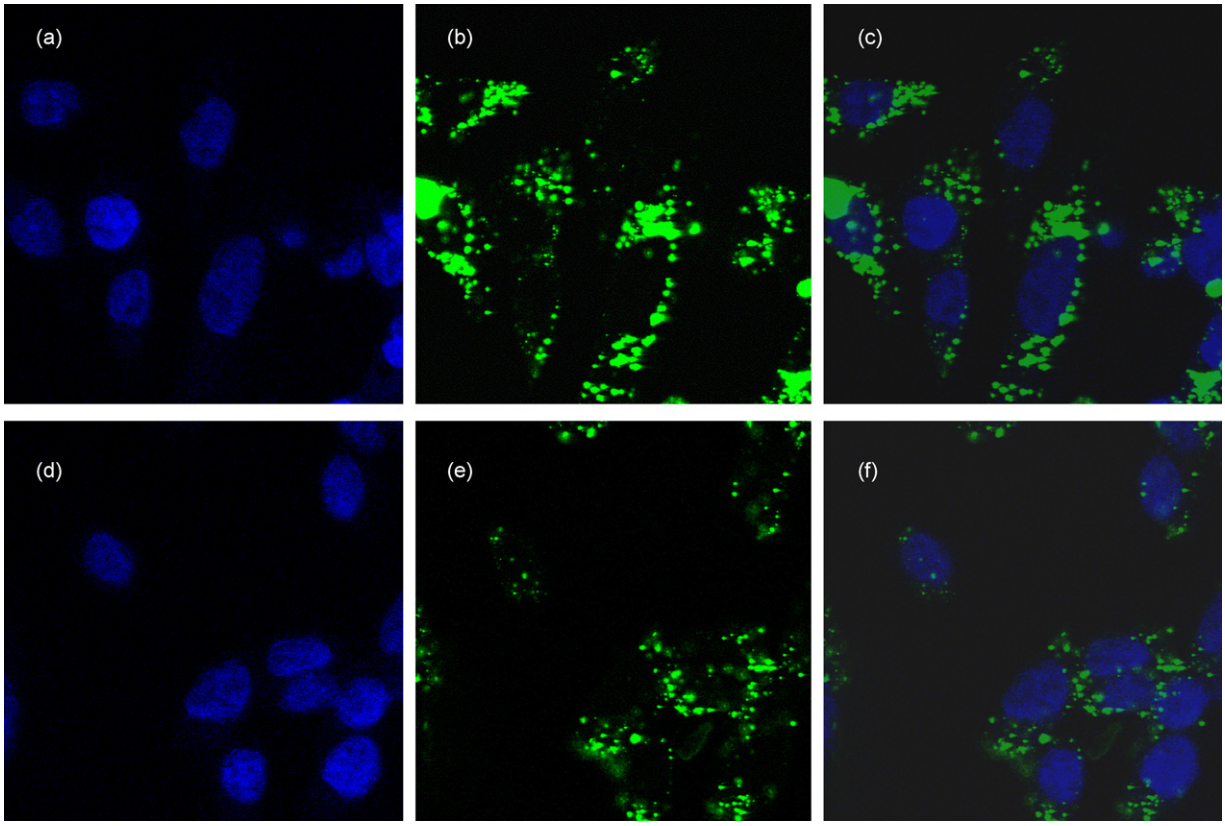

Fig. 7. Fluorescence confocal micrographs of CHO cells incubated with 50 μg mL^{-1} T-FITC-MSN (a–c) and S-FITC-MSN (d–f). (a and d) Fluorescence image excited at 340 nm to visualize the cell nuclei stained with DAPI. (b and e) Fluorescence image excited at 488 nm to visualize the FITC doped MSN that have been internalized by cells. (c and f) Overlaid micrographs of (a and b) and (d and e), respectively.

examples of enhanced uptake of cancer cells and receptor over-expressed cells over noncancerous cells [26,27].

To investigate the aggregation ability of these MSNs in aqueous solutions, the zeta potential (ζ-potential) of both materials were measured using a Malvern Nano Zetasizer to determine the surface charges that correspond to T-FITC-MSN and S-FITC-MSN. The ζ-potentials were measured to be -1.90 mV and -1.50 mV for T-FITC-MSN and S-FITC-MSN, respectively. Since the surface charges of the MSN are statistically equivalent, we assumed that endocytosis efficiency and rate were dependent exclusively upon morphology and particle aggregation. The aggregation and particle sizes were measured using a dynamic light scattering technique. Both morphologies were discovered to aggregate at 500.0 μg mL^{-1} (Fig. 6). Specifically, S-FITC-MSN showed a rather sharp peak at 712 nm, representing a small aggregation distribution while T-FITC-MSN showed a broader distribution ranging from 955 to 1480 nm. The fact that T-FITC-MSN aggregates into larger particles may be another reason for the slower cellular uptake of T-FITC-MSN.

To further investigate the cellular uptake and biocompatibility of the MSNs, CHO cells ($\sim 1 \times 10^5$ cells mL^{-1}) were incubated overnight ($\sim$12 h) with T-FITC-MSN and S-FITC-MSN (50.0 μg mL^{-1}). The first fluorescence confocal micrographs in each series (Fig. 7a and d) showed the presence of healthy, round nuclei, stained blue by 4′,6-diamidino-2-phenylindole (DAPI) and excited at 340 nm. DAPI is a blue-fluorescent dye known to complex with double-stranded DNA. Green fluorescence from T-FITC-MSN and S-FITC-MSN were observed in the cell bodies of these CHO cells in Fig. 7b and e. The DAPI and green fluorescent excited micrographs were recorded at the same focal depth. As we are able to clearly observe the nuclei, we can be assured that we are observing a focal plane that intersects the cell. The existence of oval, seemingly healthy nuclei lead us to believe that these MSN are in fact biocompatible, and do not affect the cell cycles in a detrimental way during the endocytosis process.

4. Conclusion

In summary, we demonstrated the endocytosis of MSN with spherical- and tube-like morphology in cancer and noncancerous cell lines. These MSN have unique efficiencies of endocytosis, which are both morphology and cell line dependent. We have rationalized the size and aggregation tendencies to be determining factors in endocytosis efficiency and kinetics. We envision that understanding this difference in efficiency and kinetics may allow researchers to more accurately control the rate of drug and therapeutics delivery.

Acknowledgement

The authors thank U.S. NSF (CHE-0239570), U.S. DOE, Office of Basic Energy Sciences (DE-AC02-07CH11358), and the Plant Science Institute at Iowa State University for financial support.

References

[1] J.S. Beck, J.C. Vartuli, W.J. Roth, M.E. Leonowicz, C.T. Kresge, K.D. Schmitt, C.T.W. Chu, D.H. Olson, E.W. Sheppard, et al., J. Am. Chem. Soc. 114 (1992) 10834–10843.
[2] C.T. Kresge, M.E. Leonowicz, W.J. Roth, J.C. Vartuli, J.S. Beck, Nat. (Lond.) 359 (1992) 710–712.
[3] H.-T. Chen, S. Huh, J.W. Wiench, M. Pruski, V.S.Y. Lin, J. Am. Chem. Soc. 127 (2005) 13305–13311.
[4] S. Huh, H.-T. Chen, J.W. Wiench, M. Pruski, V.S.Y. Lin, Angew. Chem., Int. Ed. 44 (2005) 1826–1830.
[5] S. Huh, H.-T. Chen, J.W. Wiench, M. Pruski, V.S.Y. Lin, J. Am. Chem. Soc. 126 (2004) 1010–1011.
[6] Z. Mehraban, F. Farzaneh, Microporous Mesoporous Mater. 88 (2006) 84–90.
[7] Y.X. Zhao, M.Y. Ding, D.P. Chen, Anal. Chim. Acta 542 (2005) 193–198.
[8] V.S.Y. Lin, C.-Y. Lai, J. Huang, S.-A. Song, S. Xu, J. Am. Chem. Soc. 123 (2001) 11510–11511.
[9] D.R. Radu, C.-Y. Lai, K. Jeftinija, E.W. Rowe, S. Jeftinija, V.S.Y. Lin, J. Am. Chem. Soc. 126 (2004) 13216–13217.
[10] C.-Y. Lai, B.G. Trewyn, D.M. Jeftinija, K. Jeftinija, S. Xu, S. Jeftinija, V.S.Y. Lin, J. Am. Chem. Soc. 125 (2003) 4451–4459.
[11] N.K. Mal, M. Fujiwara, Y. Tanaka, Nat. (Lond.) 421 (2003) 350–353.
[12] T.D. Nguyen, H.-R. Tseng, P.C. Celestre, A.H. Flood, Y. Liu, J.F. Stoddart, J.I. Zink, Proc. Natl. Acad. Sci. U.S.A. 102 (2005) 10029–10034.
[13] B.G. Trewyn, C.M. Whitman, V.S.Y. Lin, Nano Lett. 4 (2004) 2139–2143.
[14] M. Vallet-Regi, A. Ramila, R.P. del Real, J. Perez-Pariente, Chem. Mater. 13 (2001) 308–311.
[15] S. Giri, B.G. Trewyn, M.P. Stellmaker, V.S.Y. Lin, Angew Chem., Int. Ed. 44 (2005) 5038–5044.
[16] A. Ramila, B. Munoz, J. Perez-Pariente, M.J. Vallet-Regi, Sol–Gel Sci Technol. 26 (2003) 1199–1202.
[17] X. Xing, X. He, J. Peng, K. Wang, W. Tan, J. Nanosci. Nanotechnol. 5 (2005) 1688–1693.
[18] W.H. Suh, A.R. Jang, Y.-H. Suh, K.S. Suslick, Adv. Mater. (Weinheim, Germany) 18 (2006) 1832–1837.
[19] R.A. Gemeinhart, D. Luo, W.M. Saltzman, Biotechnol. Progr. 21 (2005) 532–537.
[20] C.-W. Lu, Y. Hung, J.-K. Hsiao, M. Yao, T.-H. Chung, Y.-S. Lin, S.-H. Wu, S.-C. Hsu, H.-M. Liu, C.-Y. Mou, C.-S. Yang, D.-M. Huang, Y.-C. Chen, Nano Lett. 7 (2007) 149–154.
[21] D.-M. Huang, Y. Hung, B.-S. Ko, S.-C. Hsu, W.-H. Chen, C.-L. Chien, C.-P. Tsai, C.-T. Kuo, J.-C. Kang, C.-S. Yang, C.-Y. Mou, Y.-C. Chen, FASEB J. 19 (2005) 2014–2016.
[22] Y.-S. Lin, C.-P. Tsai, H.-Y. Huang, C.-T. Kuo, Y. Hung, D.-M. Huang, Y.-C. Chen, C.-Y. Mou, Chem. Mater. 17 (2005) 4570–4573.
[23] I. Slowing, B.G. Trewyn, V.S.Y. Lin, J. Am. Chem. Soc. 128 (2006) 14792–14793.
[24] F. Torney, B.G. Trewyn, V.S.Y. Lin, K. Wang, Nat. Nanotechnol. 2 (2007) 295–300.
[25] S. Huh, J.W. Wiench, J.-C. Yoo, M. Pruski, V.S.Y. Lin, Chem. Mater. 15 (2003) 4247–4256.
[26] N. Kohler, C. Sun, J. Wang, M. Zhang, Langmuir 21 (2005) 8858–8864.
[27] I. Steinhauser, B. Spaenkuch, K. Strebhardt, K. Langer, Biomaterials 27 (2006) 4975–4983.
[28] S. Huh, J.W. Wiench, B.G. Trewyn, S. Song, M. Pruski, V.S.Y. Lin, Chem. Commun. 18 (2003) 2364–2365.